JMEPEG (2004) 13:366-373
DOI: 10.1361/10599490419216

1059-9495/$19.00

Using a Parametric Design of Two-Step Processes to Predict Quality Characteristics of Heated Treatment by the High-Density Energetic Beam

Ming-Der Jean and Jen-Ting Wang

(Submitted 23 January 2003)

This study applies the Taguchi method to elucidate the quality characteristic of the melt depth in electron beam surface treatment (EBST) of cast iron. The-nominal and the-better was a measured quality characteristic to evaluate the experimental results by computing the signal-to-noise ratios (SNRs) of the EBST melt depth after surface-hardening tests. It includes two steps to determine the optimum parameters or conditions. The first step is to maximize SNR to minimize the variance, and the second step is to adjust the EBST melt depth to a target value using the sensitivity. Results from the experiment indicate that the optimal process parameters are a substrate matrix of gray cast iron, a travel speed of 39 mm/s, an accelerating voltage of 10 kV, an electrical current of 15 mA, a melt width of 20 mm, an elliptical beam oscillation, and a post-process heat treatment at 150 °C. The best EBST melt depth obtained in the study was 0.747 mm, corresponding to the maximum SNR. The microstructure is composed of fine dendrites and martensite phases. The obtained EBST depth is confirmed by its falling into the predicted 95% confidence interval. The prediction of the optimal setting is close to the actual target value. The reproducibility of the optimal EBST parameters was experimentally established with data from the confirmation run. EBST wear-resistant surface hardening can be performed using Taguchi experiments.

Keywords analysis of variance, electron beam surface treatment, martensite, signal-to-noise ratio, the-nominal and the-better

1. Introduction

Surface treatment is presently a subject of considerable interest because it seems to offer the opportunity to yield components with idealized surface and bulk properties. Wear-resistant surfaces require a material with properties that are superior to those of the substrate to which they are applied. These properties can be developed by several competing heat treatments, ranging from the lower energy-density processes of flaming and surface induction heating to the higher energy-density processes like laser and electron beam (EB) hardening. EB hardening of a wear-resistant material is more flexible than surface induction hardening and offers more precise control than flame hardening. It does not have the reflectivity of laser hardening, however. In summary, EB surface hardening competes with welding, hardfacing, and several other surface-hardening processes, but cannot be easily used for applications in which the dimensions of the wear-resistant material are considerably limited. The use of EB hardening in any form must be properly specified. Consequently, an appropriate means of depicting EB hardening is required, such as depth and hardness of the hardened area among the specific quality characteristics.

Cast iron is difficult to surface-harden during heat treatment because it has a high carbon content and poor weldability. Several studies have been conducted, involving conventional approaches[1-4] and high-density energetic beams.[5-9] Of the heat-treated processes, EB surface treatment (EBST) has been rarely used, and the associated processing parameters have not been systematically analyzed. Therefore, the effects of process parameters on the EBST hardening of cast iron, and hence the importance of these parameters, are not yet well understood.[10-12] The complexity of this process, especially that portion associated with the interaction between the EB and the material, warrants further investigation, since this interaction produces a rapidly quenched surface layer on a metal substrate.[13] Thus, the EBST process parameters are important to establish, and the effect of the process parameters on the microstructure must be determined.

The Taguchi approach is extensively used in quality engineering. Taguchi methods were the preferred approach in the present study, since they have been effective and efficient in improving the quality of products and the performance of processes. These improvements are attained by statistically designing experiments at a relatively low cost. The Taguchi experimental method has the superior features of comparing fewer data sets with full-factorial design and efficiently reaching the optimal solution. It applies the orthogonal table and simplified analysis of variance (ANOVA) to search for the optimal significant parameters, so that deviations across the product are minimized. However, the application of Taguchi methods in EBST processes has attracted very little attention and requires further study to increase the range of industrial applications.[14-27] The goal of this study was to determine the

Ming-Der Jean, Department of Electrical Engineering, Yung-Ta Institute of Technology & Commerce, 316 Chunshan Road, Lin-Lo, Ping-Tung, Taiwan 909, Republic of China; and **Jen-Ting Wang,** Department of Mathematics, Computer Science, and Statistics, State University of New York College at Oneonta, Oneonta, NY 13820. Contact e-mail: mdjeam@mail.ytit.edu.tw.

Table 1 The Heat Source Intensities of the EBST Processes

No. of Test	1	2	3	4	5	6	7	8	9	10	11	12	13	14	15	16	17	18
Heat input, MJ/m^2	2.0	2.5	5.0	0.33	0.93	5.0	0.5	1.11	0.83	6.67	2.5	5.0	0.37	2.5	1.67	0.44	0.41	3.33

best setting of each parameter so that the EBST melted depth of the wear-resistant surface of an EB-heated specimen reaches its ideal limit.

2. EBST

2.1 High-Density Energetic Beam Heating Melted Process

EBSTs are well-developed processes that depend on high-density energetic welding technology. When EB produces the highly concentrated energy at 10^3 MJ/m^2 and penetrates the hardened specimen, it creates a keyhole effect that makes the hardened specimen well balanced, as is shown in Table 1. Figure 1 schematically depicts the basic elements of the welder. The source of the electrons is a tungsten filament, heated by a filament current power supply. The electrons are emitted and accelerate toward the anode plate. They can be focused with electromagnets and permanent magnets, which act as magnetic lenses. The permanent magnets are used to align the beam, and the electromagnets are used to focus it. The focused beam can weld, cut, or heat a specimen. The heat source in the melted surface-hardening experiment was a Sciaky (Chicago, IL) EB welder. The process was conducted in a vacuum at 10^{-5} torr to prevent collision between electrons and gas molecules, which would otherwise scatter or diffuse the EB.

An EB includes beams of high energetic intensity to yield a highly refined microstructure and to enhance the mechanical properties of the target material due to the rapidly solidified region. During the EBST process, the surface is melted to generate not only structures with properties other than those that can be obtained by conventional melting, but also generate rapid solidification that also yields regions of amorphous material. Accordingly, the proper selection of EBST process parameters can result in a very hard wear surface with little distortion and good dimensional tolerance.

2.2 Experimental EBST-Tested Conditions

The matrix material used in the EBST hardening experiments includes spherical (FCD) and gray cast iron (FC). The dominant microstructure in the castings is a pearlitic matrix with average Vickers hardness (H_v) values of 197 H_v in FCD and 245 H_v in FC. A 15 × 50 × 100 mm heated area produced by a high-density energetic beam source was used in the process. The original EBST process parameters included an FC substrate matrix, a travel speed of 10 mm/s, an accelerating voltage of 50 kV, an electrical current of 15 mA, a melted width of 15 mm, an oscillating line type, and a post-heated treatment of 25 °C. All process conditions are shown in Table 2. The specimens were cross-sectioned, polished, and then etched with a 5% Nital solution. The as-melted surfaces of process specimens were metallographically observed by optical and scanning electron microscopy with the EBST melt depth of the surface-hardened layers measured.

3. Robustness of the Taguchi Method

3.1 Selecting Control Factors and Levels

The Taguchi method was developed to improve the quality of products and processes, when that quality depends on several factors. Simple logic will usually be sufficient to establish all possible combinations of process parameters in a test-and-development strategy. The tested combinations are reduced by performing partial factorial experiments. Taguchi constructed a special set of general designs for factorial experiments with various applications. The combination of standard experimental design techniques and analytic methods in the Taguchi approach generates a consistency and reproducibility that is rarely found in other statistical methods.

Some controllable experimental testing parameters of the melted surface-hardening equipment were considered: the substrate matrix material; the speed of travel; the accelerating voltage; the electrical current; the melted width; the shape of the beam's oscillation; and the nature of the post-heated treatment. All of the factors have three levels except for the substrate matrix material, which has two levels. Based on the Taguchi experimental layout, the modified orthogonal arrays of $_{18}L(2^1 \times 3^6)$ are employed. Table 3 shows that the main effect of the layout was to reduce the minimum bias and to analyze the experimental data. The 18 rows of the L18 orthogonal arrays represent 18 experiments, much fewer than the 2×3^6 (1458) experiments in the full-factorial design. Table 3 presents the L18 orthogonal arrays, where test 1 is to be conducted with each of the seven control factors set to level 1, and so forth. The EBST melted depth with the best dimensional specification for wear-resistant surface hardening layers is 0.75-1.00 mm,[7] and the lower dimensional limit of 0.75 mm was selected.

Each experiment was performed three times to ensure accuracy. The characteristic of the Taguchi method is its efficiency, using fewer experiments to yield the same results as those from the full design.

3.2 Estimating Signal-to-Noise Ratio

In the Taguchi method, the signal-to-noise ratio (SNR) index specifies the quality characteristics. The SNR calculation shows that the mean square deviation exceeds the variance in this experiment. Their being unbalanced tends to yield an incorrect relative deviation. The-nominal and the-better formula would provide a better and reasonable estimate for the SNR. The normalized static characteristics in the basic formula of Taguchi help to explain the results. Accordingly, the modified SNR[26] is given by,

$$SNR = -10 \log \left[\frac{(y_i - m)^2}{\max_i (y_i - m)^2} + \frac{\sigma_i^2}{\max_i (\sigma_i^2)} \right] \quad \text{(Eq 1)}$$

where y_i represents the ith tested performance mean characteristics obtained from the three replications; σ_i^2 is the tested variance from the ith mean, and m is the target value of the characteristic.

3.3 ANOVA Table

From the ANOVA, significant factors can be quickly determined (i.e., the operating parameters or conditions). For a design that involves replicated experiments, Taguchi recommends that the SNR and the mean responses of the process be used to establish ANOVA tables. Consequently, the-nominal and the-better are used for the EBST process in which the goal was to approach our target value. ANOVA is performed on the experimental results to evaluate the source of variation from the EBST process. From the analysis, the most important factors can be easily identified in terms of the prespecified quality characteristic. Accordingly, these important factors must be carefully controlled during the process to ensure that the products are of consistently high quality.

4. Experimental Results and Discussion

In surface hardening, the quality characteristics of the EBST melt depth were measured experimentally and were converted into SNRs. The optimal combination of process parameters or conditions was determined by the analysis of SNR and sensitivity.

The objective of the-nominal and the-better approach is to minimize the variation around the mean and the mean close to the target value. Thus, in the two-step optimization for a nominal-better application, the first step is to maximize the SNR, and the second step is to adjust the sensitivity.

4.1 SNR Analysis of The-Nominal and The-Better

Table 4 presents the computed mean square deviation of the mean depth value, variance, and SNR of the EBST process. The response table (Table 5) and the response graph (Fig. 2) present the factor effect analysis for SNR. The experimental results show that factors C, E, and G have a stronger impact than the other factors due to their higher association with the SNR. The SNR indicates the influence of each level of each factor on the EBST depth of the hardened layers. However, the EBST depth of hardening cannot be predicted from the factors. Table 6 presents the ANOVA. The purpose of ANOVA is to determine those factors that strongly affect the EBST melt depth at a confidence level >75%. Notice that in Table 4 the specimen that was not given a post-process heat treatment in test 9 yields the largest SNR, an EBST melt depth that is nearly on target, and, correspondingly, the lowest variance. The specimen given a post-process heat treatment at 300 °C in test 3 yielded the lowest SNR, a mean EBST melt depth far from target, and, correspondingly, the largest variance. All of the

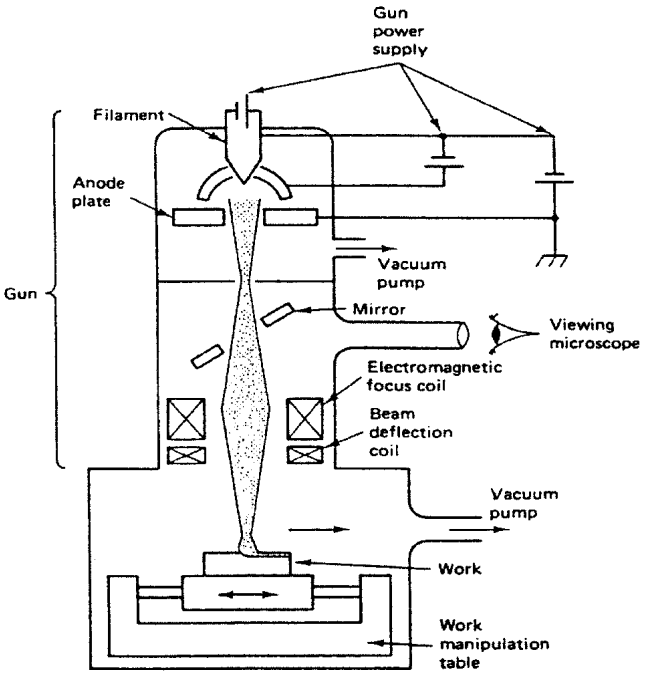

Fig. 1 Schematic of an EB system for surface-hardening treatment[7]

Table 2 Process Control Factor and Their Level

Symbol	Process Control Factor	Level 1	Level 2	Level 3
A	Substrate matrix	FCD	FC (a)	
B	Travel speed, mm/s	10 (a)	20	30
C	Accelerating voltage, kV	10	25	50 (a)
D	Electrical current, mA	10	15 (a)	20
E	Melted width, mm	5	15 (a)	20
F	Beam oscillation shape	Line (a)	Circle	Ellipse
G	Post heated treatment, °C	25 (a)	150	300

(a) Initial conditions.

EB-treated specimens are much harder than the substrate, mainly due to the rapid self-quenching effects that occur during the EBST process. Consequently, the control factor substrate matrix weakly impacts the EBST depth. Figure 3 presents plots of the relationships among the SNR, the mean EBST melt depth, and the heat input during surface hardening. It also shows a clear trend that for a low heat input in which the mean is close to the target and the SNR is high. Comparing Tables 1 and 4 also shows that the relatively low EBST melt depth in some tests is due to low thermal heat input. The combined effects of the EBST process parameters give rise to rapid solidification of the surface-hardening layer, which leads to high hardness of the wear-resistant surface.

In Table 6, the F values of factors C, E, and G exceed the critical value of F (0.25, 2, 17) = 1.51 at $\alpha = 0.25$ significance level. Hence, from Table 5 and Fig. 2, factor C (the accelerating voltage), factor E (the melted width), and factor G (the post-heated treatment) are confirmed as having major effects on functional variability. The other factors (A, B, D, and F) have minor effects. Consequently, the combination of levels, A_1, B_3, C_1, D_2, E_3, F_2, and G_2 are selected to yield the maximum SNR.

Table 3 The Experimental Layout, Results, and Replications

Test No.	Process Control Factor							EBST Depth, mm		
	A	B	C	D	E	F	G	N1	N2	N3
1	1	1	1	1	1	1	1	2.14	2.23	2.29
2	1	1	2	2	2	2	2	1.06	1.12	1.11
3	1	1	3	3	3	3	3	2.21	2.13	2.06
4	1	2	1	1	2	2	3	0.45	0.56	0.53
5	1	2	2	2	3	3	1	0.75	0.73	0.81
6	1	2	3	3	1	1	2	2.83	3.12	3.05
7	1	3	1	2	1	3	2	0.81	0.92	0.94
8	1	3	2	3	2	1	3	1.2	1.13	1.29
9	1	3	3	1	3	2	1	0.82	0.85	0.79
10	2	1	1	3	3	2	2	0.54	0.61	0.58
11	2	1	2	1	1	3	3	2.31	2.46	2.29
12	2	1	3	2	2	1	1	1.16	1.23	1.08
13	2	2	1	2	3	1	3	0.32	0.37	0.40
14	2	2	2	3	1	2	1	2.35	2.29	2.56
15	2	2	3	1	2	3	2	0.82	0.89	0.92
16	2	3	1	3	2	3	1	0.26	0.29	0.31
17	2	3	2	1	3	1	2	0.29	0.31	0.39
18	2	3	3	2	1	2	3	2.52	2.83	2.46

Table 4 The EBST Processing SNRs for Each Test

Test No.	Mean	MSD (a)	Variance	SNR	Test No.	Mean	MSD	Variance	SNR
1	2.220	2.1609	0.00570	2.43	10	0.576	0.0300	0.00123	14.29
2	1.096	0.1202	0.00103	13.02	11	2.353	2.5707	0.00863	1.39
3	2.133	1.9136	0.00563	2.83	12	1.156	0.1654	0.00563	7.56
4	0.513	0.0560	0.00323	10.31	13	0.364	0.1495	0.00163	11.49
5	0.763	0.0002	0.00173	13.57	14	2.401	2.7225	0.02010	–0.20
6	3.000	5.0625	0.02290	–1.99	15	0.876	0.0160	0.00263	11.55
7	0.891	0.0196	0.00490	8.92	16	0.286	0.2147	0.00063	12.33
8	1.206	0.2085	0.00643	6.90	17	0.331	0.1764	0.00280	9.75
9	0.822	0.0049	0.00090	16.24	18	2.603	3.4348	0.03943	–2.25

(a) MSD = mean standard deviation.

4.2 Sensitivity Analysis of The-Nominal and The-Better

In the EBST process, the EBST melt depth is a finite target. The mean value of a quality characteristic is defined using sensitivity factors. Table 7 presents a response table, and Fig. 4 presents a response graph that together represent a factorial effect analysis. According to this factor effect analysis, the combination of levels A_1, B_1, C_3, D_3, E_1, F_1, and G_3 maximizes the sensitivity. Therefore, a variance analysis is used to confirm the major effect factor at a 95% confidence level. Table 8 indicates a comparison between the F values or contribution percentages in the ANOVA. The F values of B (travel speed), C (accelerating voltage), D (electrical current), E (melt width), and G (post-process heat treatment) exceed the critical value of $F(0.05, 2, 17) = 3.59$ at $\alpha = 0.05$ significance level. So, factor B, factor C, factor D, factor E, and factor G meet this requirement. These factors are seen to have a major effect on the sensitivity. The other factors (A and F) have a minor effect. In reducing the variability by maximizing SNR, factors B and D are significant for sensitivity and are selected as adjustable factors. The performance EBST melt depth can be adjusted to near the ideal hardening depth. From the experimental results, factors B_3 (30 mm/s travel speed) and D_2 (15 mA electrical current) are selected as coarsely adjustable factors in the optimization. Additionally, for economic reasons, A_2 (gray cast iron) and F_3 (elliptical shape) are selected. A_2 is selected to maximize the quality of the process due to its having more complete hardening and less deformation, and F_3 is selected to reduce the cost of the operating process because it yields less surface roughness of the hardening layers and a smoother surface. Therefore, the combination A_2, B_3, C_1, D_2, E_3, F_3, and G_2 yields the optimal result. Even so, the EBST melt depth is still as high as 0.792 mm. Consequently, a fine adjustment should be made. For example, an adequate electrical current factor D_2 (15 mA electrical current) is selected, and then factor B (travel speed) is used to adjust the maneuverability of the factorial level. The response graph (Fig. 2) shows that travel speed has linear levels. The EBST melt depth is adjusted by the method of extrapolation, which requires that B_4 should be set at $B_3 + 25/57 (B_3 - B_1)$ and the travel speed close to 39 mm/s. Now, the SNR can remain maximized, and the EBST melt depth could be adjusted to the target value using the sensitivity. After optimization in two steps, the final combination of processing parameters is A_2, B_4, C_1, D_2, E_3, F_3, and G_2. That is, a substrate matrix of gray cast iron, a travel speed of 39 mm/s, an accelerating voltage of 10 kV, an electrical current of 15 mA, a melted width of 20 mm, an elliptical beam oscillation, and post-heated treatment at 150 °C are used.

Table 5 The SNRs for Each Control Factor and Their Comparisons

Factor	A	B	C	D	E	F	G
Level 1	8.02	6.92	9.96	8.61	1.38	6.02	8.65
Level 2	7.32	7.46	7.40	8.72	10.28	8.57	9.26
Level 3	…	8.65	5.66	5.69	11.36	8.43	5.11
Max-min	0.70	1.73	4.31	3.02	9.98	2.54	4.15

Table 6 The ANOVA Table for SNR

Symbol	Sum of Squares	DOF (a)	Variance	F-ratio	Contribution Percentage
A	2.2	1	2.214	0.212	0.376
B	9.4	2	4.702	0.451	1.595
C	56.3	2	28.156	2.701	9.553
D	35.3	2	17.665	1.694	5.994
E	359.7	2	179.845	17.251	61.022
F	24.6	2	12.296	1.179	4.172
G	60.2	2	30.103	2.888	10.214
Error	41.7	4	10.425	1.000	7.074
Total	589.4	17	34.673	…	100.000

(a) DOF = degrees of freedom.

4.3 Estimation and Prediction

According to the Taguchi method, the control factor levels that yield the highest SNR response are selected as the optimal configuration. According to the factorial level response effect, the performance with the optimal combination parameters developed in two-step experiments can be determined by adding significant factor effects. The predictions of SNR and sensitivity for the optimal combination of process parameters can be determined by means of the additivity law as follows.

$$\eta_{optimum} = A_2 + B_3 + C_1 + D_2 + E_3 + F_3 + G_2 - 6\overline{T} = 7.32 + 8.65 + 9.96 + 8.72 + 11.36 + 8.43 + 9.26 - 6 \times 7.76 = 17.14 \text{ db} \quad \text{(Eq 2)}$$

$$S_{optimum} = A_2 + B_3 + C_1 + D_2 + E_3 + F_3 + G_2 - 6\overline{T} = 1.22 + 1.02 + 0.81 + 1.15 + 0.83 + 1.22 + 1.12 - 6 \times 1.06 = 1.01 \text{ mm} \quad \text{(Eq 3)}$$

Since A2, B1, C3, D2, E2, F1, and G1 are of the original design, their SNR and sensitivity are calculated as

$$\eta_{original} = A_2 + B_1 + C_3 + D_2 + E_2 + F_1 + G_1 - 6\overline{T} = 7.32 + 6.92 + 5.66 + 8.72 + 10.28 + 6.02 + 8.65 - 6 \times 7.76 = 7.01 \text{ db} \quad \text{(Eq 4)}$$

$$S_{original} = A_2 + B_1 + C_3 + D_2 + E_2 + F_1 + G_1 - 6\overline{T} = 1.22 + 1.59 + 1.77 + 1.15 + 0.88 + 1.38 + 1.27 - 6 \times 1.06 = 2.90 \text{ m} \quad \text{(Eq 5)}$$

Consequently, a 10.13 db gain in the SNR and a sensitivity of 1.01 mm are predicted.

4.4 ANOVA

Table 6 presents the ANOVA for the experimental results. ANOVA is performed on an SNR that will identify a few significant factors to be optimized for all process parameters, or factors, and subsequently to reduce variation. Factors C (accelerating voltage), E (melt width), and G (post-process heat treatment) can thus be easily seen to be the most significant in terms of process robustness. The higher the factorial contribution percentages and then the process controllable factors (parameters) are, the better are the important factors for the experimental tested results. These factors together explain almost 81% of the experimental variance, while the melt width explains the largest part. The observations agree closely with those in Fig. 2. ANOVA performs almost the same function as shown in Fig. 2, except that it provides more detailed information.

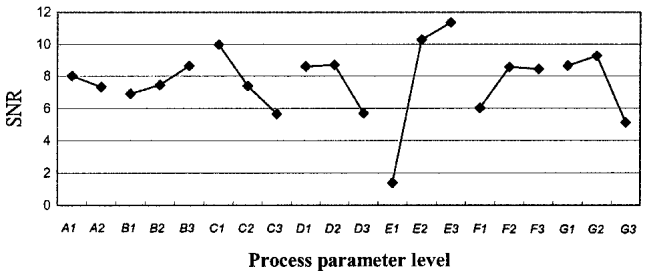

Fig. 2 The response SNR graph of the EBST melted depth

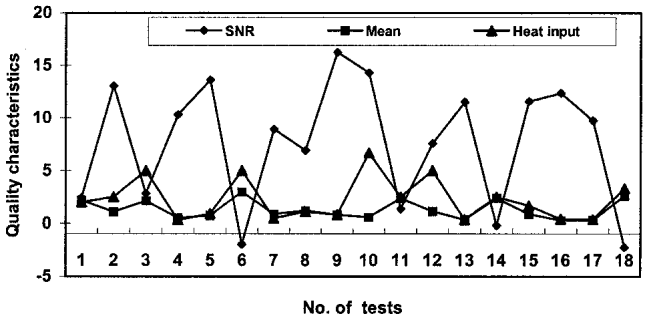

Fig. 3 The experimental results of SNR, mean, and heat input

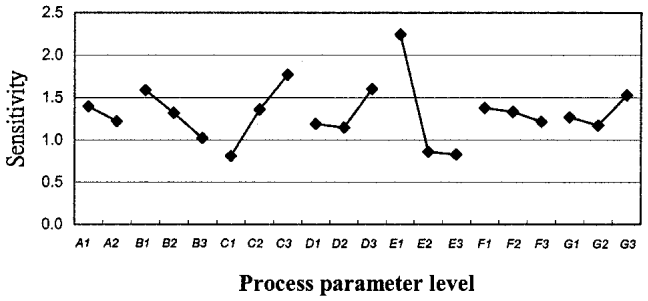

Fig. 4 Response sensitivity processing graph

Table 7 Response Sensitivity Processing Effects

Factor	A	B	C	D	E	F	G
Level 1	1.40	1.59	0.81	1.19	2.24	1.38	1.27
Level 2	1.22	1.32	1.36	1.15	0.86	1.34	1.12
Level 3	…	1.02	1.77	1.60	0.83	1.22	1.53
Max-min	0.19	0.57	0.96	0.45	1.41	0.16	0.41

Table 8 ANOVA Table for Sensitivity

Symbol	Sum of Squares	DOF (a)	Variance	F	Contribution %
A	0.160	1	0.160	2.333	1.195
B	0.964	2	0.482	7.036	7.211
C	2.766	2	1.383	20.184	20.686
D	0.761	2	0.381	5.558	5.696
E	7.851	2	3.925	57.297	58.721
F	0.084	2	0.042	0.616	0.631
G	0.509	2	0.255	3.718	3.810
Error	0.274	4	0.069	…	2.050
Total	13.369	17	0.786	…	100.000

(a) DOF = degrees of freedom.

4.5 Confirmation Run

Table 9 presents data from the confirmation run and compares them to their corresponding predicted values. There are three observed EBST melted depths under the original procedure and six for the two-step procedure. The results validate the approach. Experimental results indicate that the actual gain in SNR is 15.67 db closer to the prediction, as shown in Table 10. Clearly, this result confirms the excellent additivity and reproducibility, which provide sufficient confidence in the observed factorial effects. These factorial effects in an additive manner can therefore be reproduced additively. Accordingly, an improvement of over 15 db in SNR was expected, which is equivalent to a reduction of 97.32% in the variance, or of 83.64% in the standard deviation. This implies that the process robustness was improved 6.112 times. Figure 5 presents the distributions of quality characteristics of the surface-hardened specimens using the original and two-step optimal parametric design. The mean melt depth for both the coarse and fine-tuning optimal design experiments shifts toward the left from 1.156-0.747 mm, demonstrating a significant improvement in the EBST process. Notably, the SNR of melting depth for the two-step optimal design is further enhanced 2.07 times. The standard deviation of the quality characteristic is found to fall from 0.075-0.014 mm after the two-step optimization experiments shown in Table 9. Besides, in Fig. 5 the coarse solid curve, which has the narrowest half-width, indicates that the optimal design with fine-tuning has the minimum variation. To summarize, the process parameters, after adjustment, result in minimum variation and a mean that is closer to the target value in the two-step optimal design.

We can obtain a statistical confidence interval (CI) to find out whether the optimal process setting yields robustness within an ideal target range for the EBST melt depth of the hardened layers. At a 100(1-α)% confidence level, the CI for the target of the EBST processing depth[26] is calculated using:

$$CI = \pm \sqrt{\frac{F_{\alpha;\nu_1;\nu_2} V_e}{m_e}} \quad \text{(Eq 6)}$$

where V_e, the mean squared error under the ANOVA in Table 8, is the variance of the random *errors, ν_2 is the degree of freedom of V_e, $F_{\alpha};\nu_1;\nu_2$ represents the F ratio with degrees of freedom 1 and ν_2 at the levelα, and m_e is the effective test size. The F value at the 95% confidence level with degrees of freedom 1 and 13 is 4.67, and m_e is 3.6. Therefore, the CI yielded as ±0.2991 mm. That is, the resultant EBST melt depth after sensitivity adjustment, m = 0.747 mm, lies between 0.4509 and 1.0491 mm at the 95% confidence level.

4.6 Microstructure Analysis

After two-step optimization, the EBST melt depth is approximately the target value, as shown in Fig. 5. This result proves that the-nominal and the-better can be applied in this experiment and that the parameters under the optimal conditions can also be used. However, a microstructural analysis of the hardened layers can also be performed to verify the optimum conditions for the EBST process. Figure 6 presents the extremely fine dendritic structures at a mean EBST melt depth of approximately 0.747 mm. Due to the heating cycle effect, the EBST hardened layers have three zones: a melt zone; a partially melted zone; and a heat-affected zone. The melt zone is almost an extremely fine ledeburite structure with little residual graphite. Figure 7 magnifies this zone, showing white carbides (Fe_3C). The hardness increases to 850 H_v.[23] This high hardness gives the potential for high wear resistance.

The partially melted zone is adjacent to the melt zone and is shown as a dark gray region. Figure 8 magnifies the refined residual graphite. This region has a complex microstructure including a large disordered area of ledeburite and a chill inverse microstructure shaped liked an umbrella. The white area shows a minute amount of martensite.

The heat-affected zone is shown as a fine, dark-gray area and is composed of minute portions of martensite in the vicinity of flake graphite. Figure 9 shows plate martensite with embedded graphite. Because of the rapid solidification of hardened layers after self-quenching, the flake graphite with high carbon content causes fast carbon diffusion, which greatly transforms the matrix. Most of the carbon near the flake graphite does not diffuse.

5. Conclusions

The application of Taguchi methods was shown to be a simple, effective, and efficient way of developing a high-

Table 9 Comparison of SNRs Between the Predicted and the Confirmation Runs

Level Combination	EBST Depth, mm			Mean, mm	S (a)	SNR, db	
						Actual	Predicted
Original	1.16	1.23	1.08	1.156	0.075	7.56	7.01
Coarse tuning	0.82	0.81	0.79	0.792	0.021	19.19	17.14
	0.76	0.78	0.79				
Fine tuning	0.76	0.73	0.74	0.747	0.014	23.23	16.70
	0.75	0.74	0.76				

(a) S = sensitivity.

Table 10 Comparison of SNRs and Sensitivities

Level Combination	SNR, db		Sensitivity, mm	
	Predicted	Actual	Predicted	Actual
Original	7.01	7.56	2.90	1.16
Coarse tuning	17.14	19.19	1.01	0.792
Fine tuning	16.70	23.23	0.75	0.747
Gain	9.69	15.67	…	…

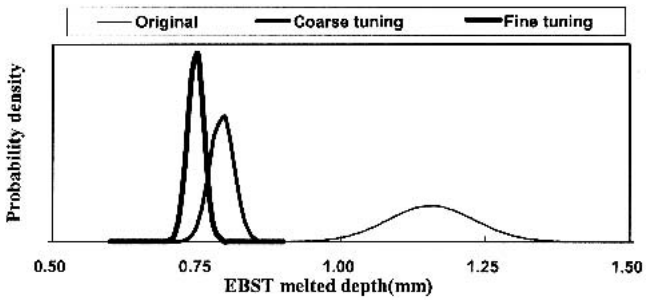

Fig. 5 Quality characteristic distribution of the original, and the tuning experiments from two-step optimal processes

quality EBST surface-hardening process. The-nominal and the-better was optimized by considering the SNR that maximizes robustness and sensitivity in order to adjust the mean to the target. This optimization was achieved in two-step experiments. The experimental results support the following conclusions.

1) The most important factors that affect the EBST melt depth of hardened layers were identified as the electrical current, the melt width, and the post-process heat treatment for the SNR, the travel speed, and the electrical current for the sensitivity.
2) The following factor settings were identified to yield the best combinations of process parameters or conditions: factor A, level 2; factor B, level 4; factor C, level 1; factor D, level 2; factor E, level 3; factor F, level 3; and factor G, level 2.
3) A gain in SNR of 9.69 db was predicted, and 15.67 db was confirmed. While this result is not perfect, it shows excellent reproducibility and verifies the success of the experiment.
4) A gain of 15.67 db can reduce the variance of the EBST depth by 97.32%. It implies that the process robustness was improved 6.112 times. A travel speed factor of 39 mm/s and an electrical current factor of 15 mA are the ideal adjustment factors or conditions. The EBST melted depth of hardened layers was adjusted optimally to reach the target value.
5) The EBST wear-resistant specimens exhibited good hardening, as evidenced by the microscopic examination of microstructures for the EBST melt depth of the hardened layers. A group of fine microstructures developed such that primary dendrites and residual graphite in the melt zone and in the partially melted zone was in the form of fine lede-

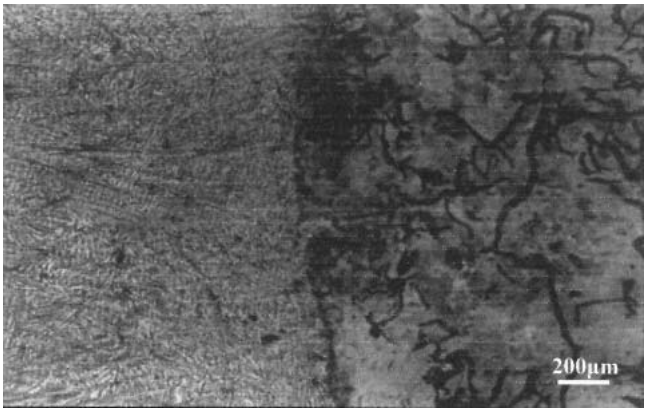

Fig. 6 Microstructure of the cross-sectioned layers, in which the mean EBST depth is close to the target value in the optimal processing parameters or conditions

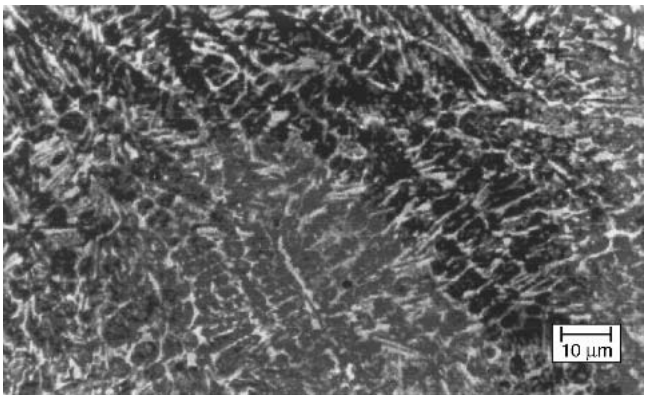

Fig. 7 Magnified microstructure of melted zone in the EBST process

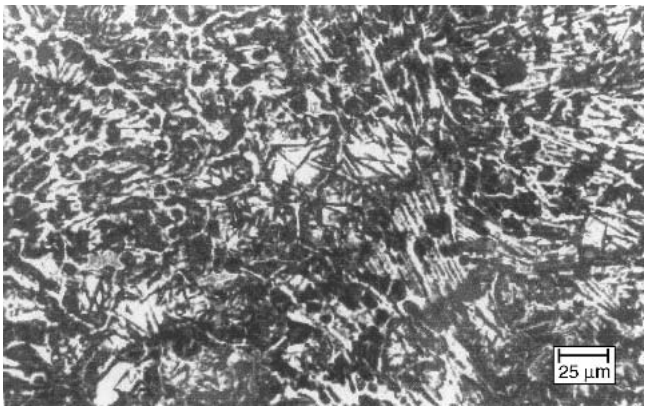

Fig. 8 Microstructures of the partial melted zone, nearly melted line

Fig. 9 Microstructures of the heat-affected zone, not melted

burite (Fe_3C), refined residual graphite, and minute amounts of martensite. The microstructure in the heat-affected zone consists of plate martensite with smaller quantities of martensite and flake graphite.

References

1. R. Creal: "High Intensity Induction: Alternate to Laser, Electron Beam," *Heat Treating,* 1982, *3*, pp. 21-8.
2. N.A. Tape, E.A. Baker, and B.C. Jackson: "Evaluation of Wear Properties of Electroles Nickel," *Plating Surf. Finishing*, 1976, *63*, pp. 30-7.
3. T.J. Kelly: "Welding Ductile Iron With Ni-Fe-Mn Filler Metals," *Welding J.*, 1985, *64*, pp. 79-85.
4. A.F. Leatherman and D.E. Stutz: "Basic Induction Heating Principles," *Solid State Technol.*, 1967, *11*, pp. 41-52.
5. R. Backish: "Electron Beam Melting, Refining and Heat Treatment," *Indust. Heating*, 1985, *6*, pp. 26-30.
6. T. Ishida: "A Microstructural Study of Local Melting Gray Cast Iron with a Stationary Plasma Arc," *Welding J.*, 1985, *64*, pp. 232-41.
7. G. Kenneth: *Surface Engineering for Wear Resistance*, Prentice Hall, Englewood Cliffs, NJ, 1988.
8. I. Atsushi: "Transformations Hardening by Electron Beam," *Bull. Japan Soc. Precision Eng.*, 1984, *18*(3), pp. 219-24.
9. A.K. Mathur and P.A. Molian: "Laser Heat Treatment of Cast Iron-Optimization of Process Variables: Part I," *J. Eng. Mater. Technol.*, 1986, *108*, pp. 233-39.
10. J.B. Jenkins: "Some Factors that Influence Electron Beam Hardening," *Heat Treating*, 1981, *2*, pp. 28-32.
11. D.A. Schauer and W.H. Giedt: "Prediction of Electron Beam Welding Spiking Tendency," *Welding J.*, 1978, *56*, pp. 183-95.
12. R. Zenker, M. Muller, and M. Murawski: "Electron Beam Hardening," *Heat Treat. Metals*, 1988, *5*, pp. 79-88.
13. M. Cohen, B.H. Kear, and R. Mehrabian: "Rapid Solidification Processing—An Outlook," in *Proc. Second International Conference on Rapid Solidification Processing*, Reston, VA, March 23-26, 1980, pp. 1-23.
14. K.N. Otto and E.K. Antonsson: "Extensions to the Taguchi Method of Product Design," *J. Mech. Design*, 1993, *115*, pp. 5-13.
15. A. Jeang and C.L. Chang: "Combined Robust Parameter and Tolerance Design Using Orthogonal Arrays," *Int. J. Adv. Manufacturing Technol.*, 2002, *19*, pp. 442-47.
16. G. Taguchi, *System of Experimental Design, 1-2*. American Supplier Institute Inc, Livonia, MI, 1993, pp. 122-56.
17. D.M. Steiberg and D. Bursztyn: "Dispersion Effects in Robust-design Experiments with Noise Factors," *J. Quality Technol.*, 1994, *26*(1), pp. 12-20.
18. J.E. Savage: "Adding Wear Resistance via Ion Implantation," *Metal Prog.*, 1984, *126*, pp. 41-4.
19. P.W. Mason and P.S. Prevey: "Optimizing the Austenite Content and Hardness in 52100 Steel," *J. Mater. Eng. Performance*, 2001, *10*(1), pp. 14-21.
20. I.S. Kim, C.E. Park, and Y.J. Jeong: "Development of an Intelligent System for Selection of the Process Variables in Gas Metal Arc Welding Processes," *Int. J. Adv. Manufacturing Technol.*, 2001, *18*, pp. 98-102.
21. Y. Matsumoto, M.M. Barash, and C.R. Liu: "Effect of Hardness on the Surface Integrity of AISI 4340 Steel," *J. Eng. Industry*, 1986, *108*, pp. 167-75.
22. T.A. Theodore and G.P. Maul: "A Method for Robust Process Design Based on Direct Minimization of Expected Loss Applied to Arc Welding," *J. Manufacturing Syst.*, 2001, *20*(5), pp. 329-48.
23. M.D. Jean: "The Study of Weldability of the Hardening Layer of the FC25 Gray Cast Iron," *Welding Cutting*, 2000, 10(6), pp. 76-84.
24. C.Y. Wu and Y.C. Hsu: "Shape Optimization of Extrusion Forging Die Using Taguchi Experiment Method," *J. Technol.*, 2001, *16*(4), pp. 657-64.
25. Y.S. Tarng, W.H. Yang, and S.C. Juang: "The Use of Fuzzy Logic in the Taguchi Method for the Optimization of the Submerged Arc Welding Process," *Int. J. Adv. Manufacturing Technol.*, 1999, *16*, pp. 668-74.
26. W. Yuin and W. Alan, *Taguchi Methods for Robust Design*, American Society of Mechanical Engineers, New York, NY, 2000, pp. 97-177.
27. S.C. Chi and L.C. Hsu: "A Fuzzy Basic Function Neural Network for Predicting Multiple Quality Characteristics of Plasma Arc Welding," *Proc. IEEE*, 2001, *89*, pp. 2807-12.